https://doi.org/10.1007/s11467-023-1331-1 Front. Phys. 19(1), 13202 (2024)

RESEARCH ARTILCE

A high-speed true random number generator based on Ag/SiN$_x$/n-Si memristor

Xiaobing Yan[#,†], Zixuan Zhang[#], Zhiyuan Guan[#], Ziliang Fang, Yinxing Zhang, Jianhui Zhao, Jiameng Sun, Xu Han, Jiangzhen Niu, Lulu Wang, Xiaotong Jia, Yiduo Shao, Zhen Zhao, zhenqiang Guo, Bing Bai

Institute of Life Science and Green Development, Key Laboratory of Brain-Like Neuromorphic Devices and Systems of Hebei Province, College of Electron and Information Engineering, Hebei University, Baoding 071002, China

[#] There authors contributed equally to the work.

Corresponding author. E-mail: [†]yanxiaobing@ime.ac.cn

Received April 1, 2023; accepted June 14, 2023

Supporting Information

When we chose a new fresh device with a larger I_{cc} (10^{-4} A), it is clearly shown that the current abruptly increased from a very small current (10^{-9} A) to the I_{cc} at 3.25 V, meaning that the electroforming process also exited in Fig. S1(c). After this electroforming process, a bipolar typical resistance switching phenomena is found and shown in Fig. S1(d), where these arrows indicate the 0 → 2.5 V→ 0 → −2.5 V → 0 voltage sweeping directions. In the bipolar resistive switching characters, the memristor retains HRS in the initial state (from 0 to 2.15 V). Then, the resistance state was abruptly transformed from the HRS to LRS at a voltage of 2.15 V. And then, with the reverse directions, the device was switched from LRS to HRS at the voltage of −2.1 V.

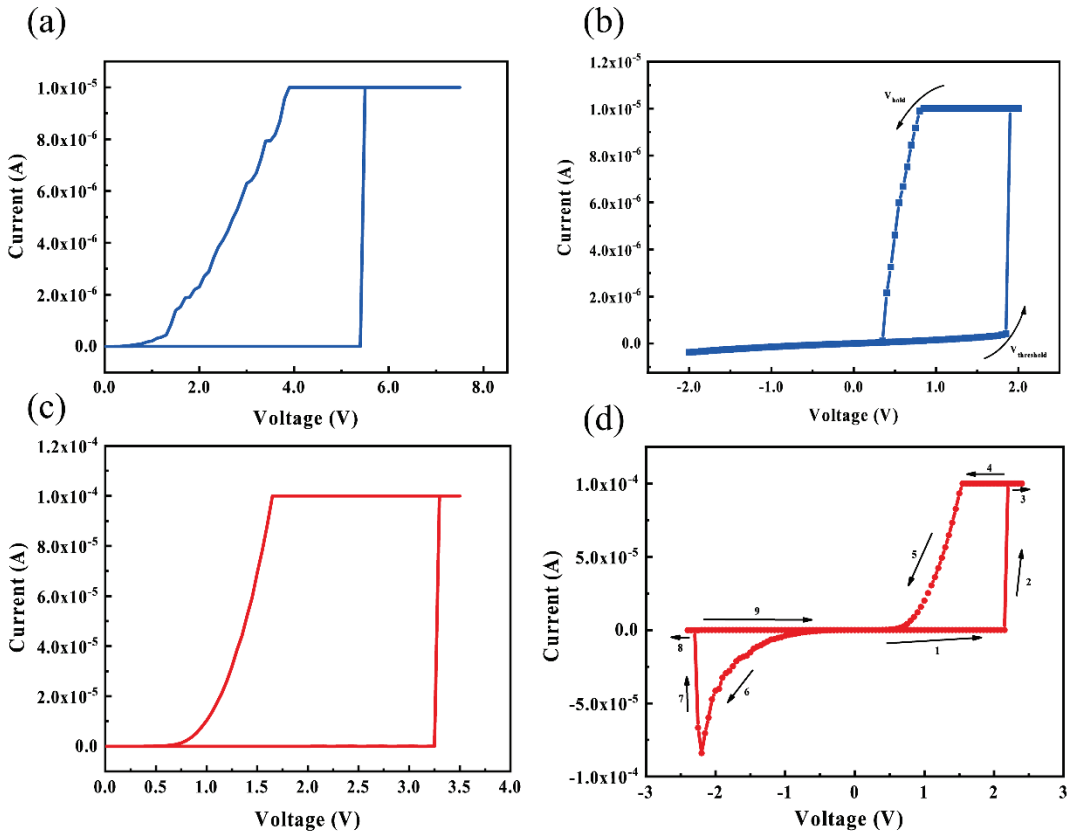

Fig. S1 (a) The electroforming process with the I_{cc} of 10^{-5} A. **(b)** The *I–V* cycle presents the threshold switching with the I_{cc} of 10^{-5} A. **(c)** The electroforming process with the I_{cc} of 10^{-4} A. **(d)** The *I–V* cycle presents the bipolar resistive switching characters with the I_{cc} of 10^{-4} A.

Figure S2(a) shows a schematic diagram of the Ag conductive filament formation and fracture process, in the absence of a voltage applied, almost no Ag^+ ionized from the silver electrode to the SiN_x layer, the device is still in HRS, when a positive voltage is applied to the top electrode of the device, the Ag atoms in the top electrode will be ionized into Ag^+ at the Ag/SiN_x interface, these Ag^+ drift to the Si electrode and diffuse into the SiN_x film, as shown in Fig. S2(b), because the Ag CFs have not yet formed, so the device is still in HRS. As the positive bias voltage of the device increases greater than V_{th}, Ag CFs are fully formed, as shown in Fig. S2(c), the formation of CFs significantly reduces the resistance of the device, and the device changes from HRS to LRS [1-3]. Due to the smaller size of the conductive filaments formed at lower currents and fewer metal bonds, the insufficient binding force of the metal atoms leads to the formation of Ag^+ that form CFs when the applied voltage is less than V_h [4], which may move through the defect site in the SiN_x layer by diffusion, resulting in the rupture of the Ag CFs allowing the device to return to HRS, as shown in Fig. S2(d). Due to the high diffusion rate of metal atoms in the electrolyte, rapid dissolution of conductive filaments may occur, thus exhibiting threshold switching behavior [5].

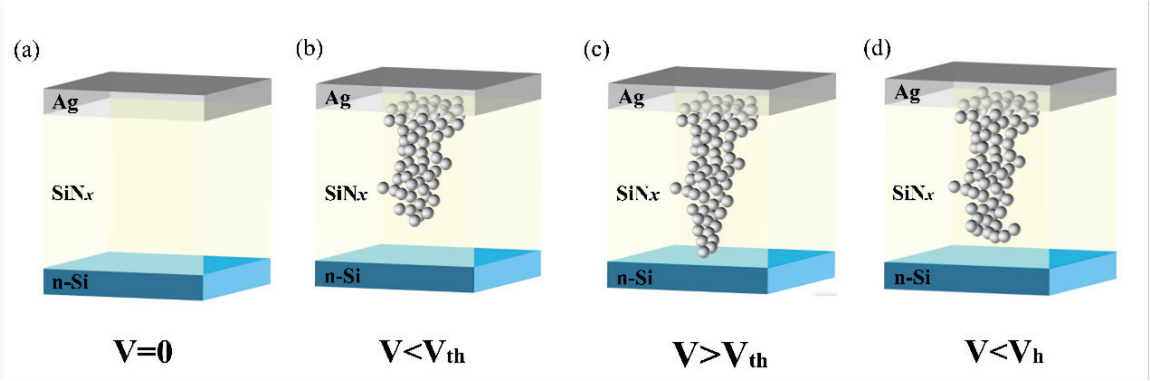

Fig. S2 (a-d) Diagram of switching dynamics in Ag/SiN_x/n-Si device.

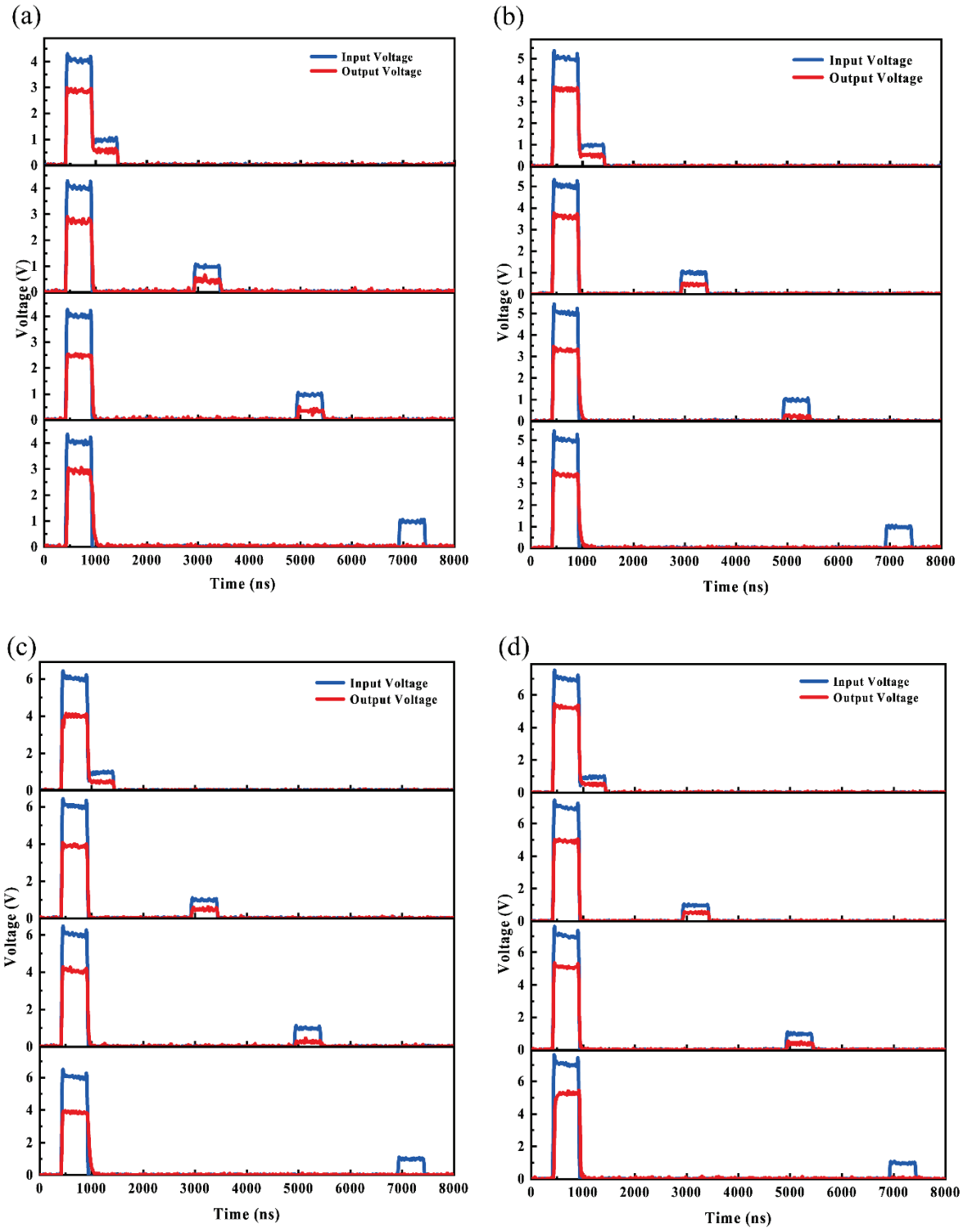

Fig. S3 (a-d) The relaxation and retention stimulated by voltage pulses (4 V, 5 V, 6 V, 7 V).

An exponential decay equation is used to describe the relaxation time of TS device:

$M(t)= M_e + (M_0-M_e) \exp(t/\tau)$.

Here, M_0 is the initial memory state, M_e is the steady state of memory, and τ is the time constant of the relaxation process [6]. It can be observed from Fig. S4(a) that the relaxation time of the device is 38 ns. In order to further explore the factors affecting the relaxation time, it is found that the relaxation time will increase with the increase of voltage or pulse width from a statistical point of view when testing according to different voltages and pulse widths as shown in the Figs. S4(b) and (c). Higher voltage amplitude or longer pulse duration time could contribute to the formation of conductive filaments which became more difficult to rupture, leading to a longer relaxation time [7].

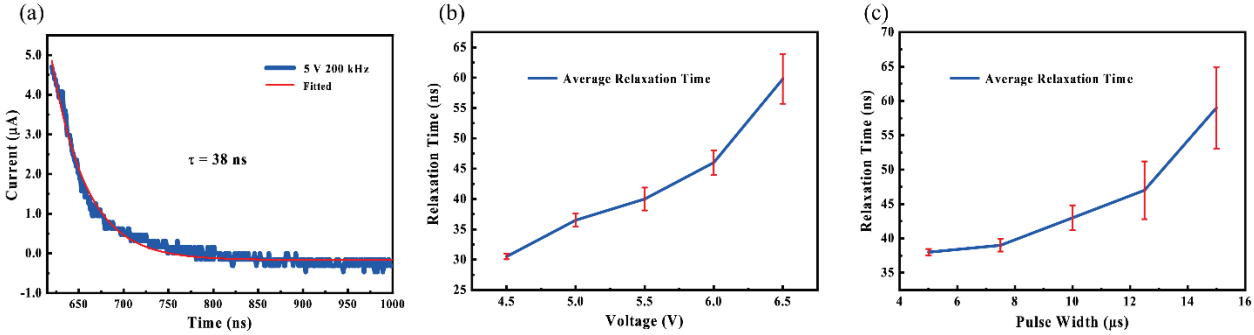

Fig. S4 (a) The relaxation time of Ag/SiN$_x$/n-Si. **(b)** The relationship of relaxation time and pulse width of Ag/SiN$_x$/n-Si. **(c)** The relationship of relaxation time and voltage amplitude of Ag/SiN$_x$/n-Si.

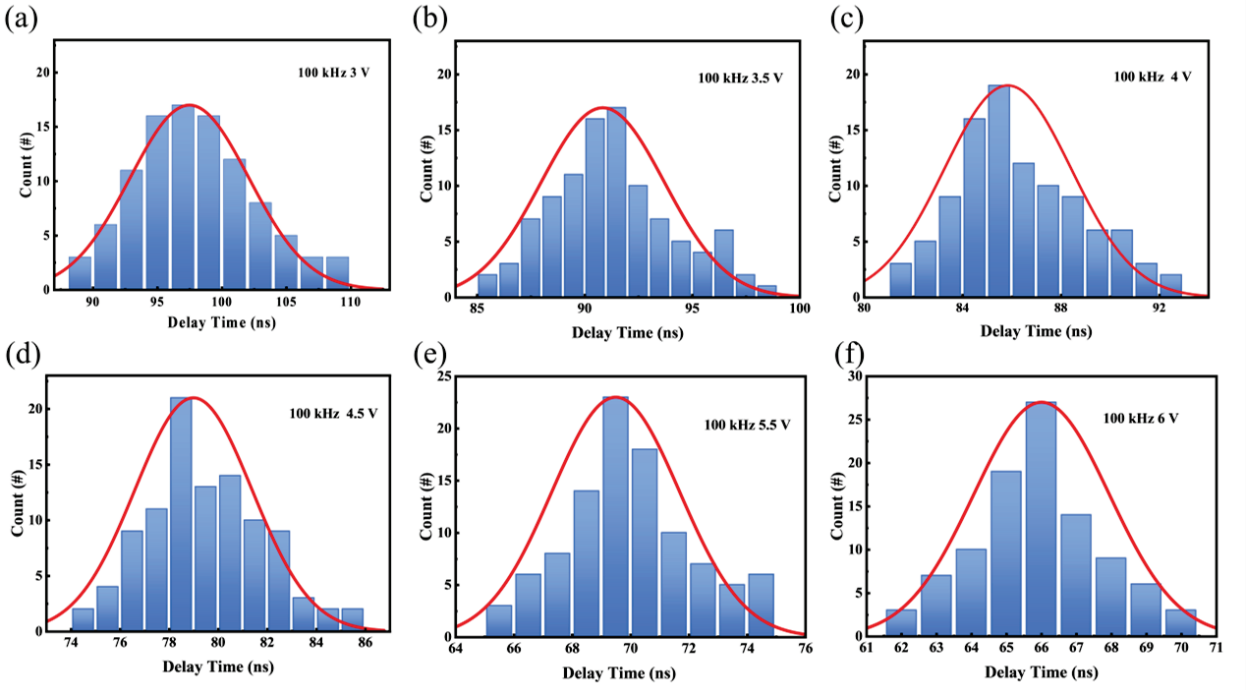

Fig. S5 A statistical diagram of different voltages (3 V, 3.5 V, 4 V, 4.5 V, 5.5 V and 6 V) and delay times at pulses with a frequency of 100 kHz.

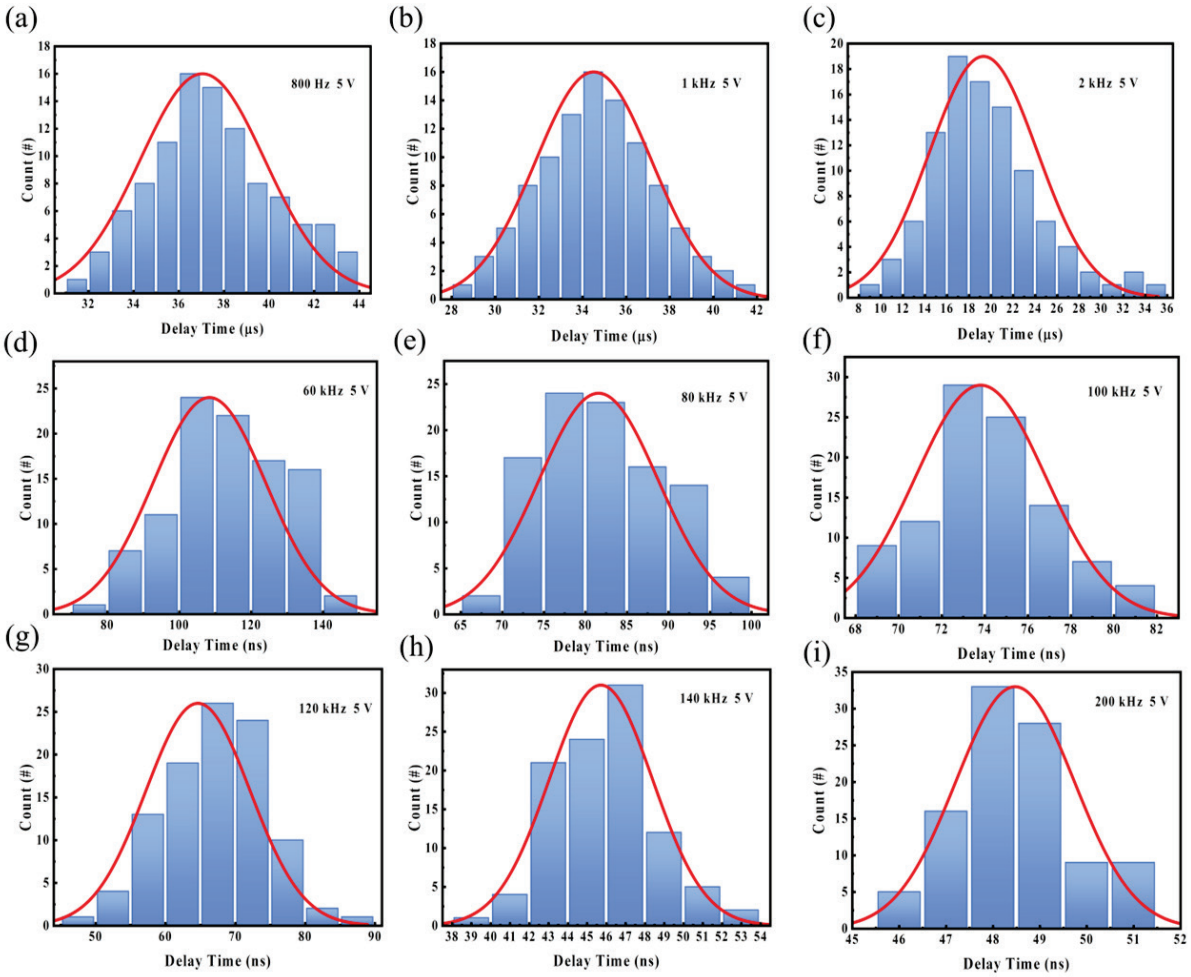

Fig. S6 A statistical diagram of different frequency (800 Hz, 1 kHz, 2 kHz, 60 kHz, 80 kHz, 100 kHz, 120 kHz, 140 kHz, 200 kHz) and delay times at pulses with a voltage of 5 V.

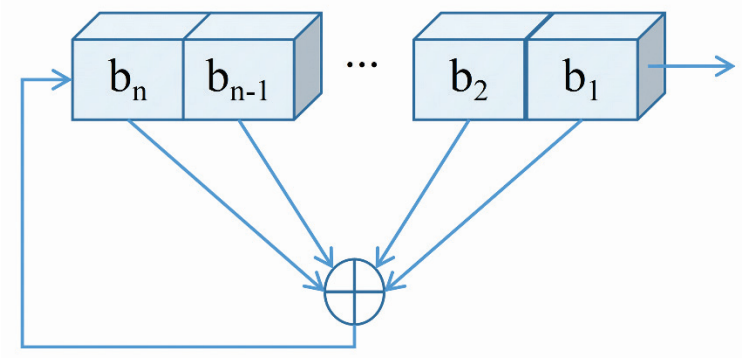

Fig. S7 n-bit LFSR.

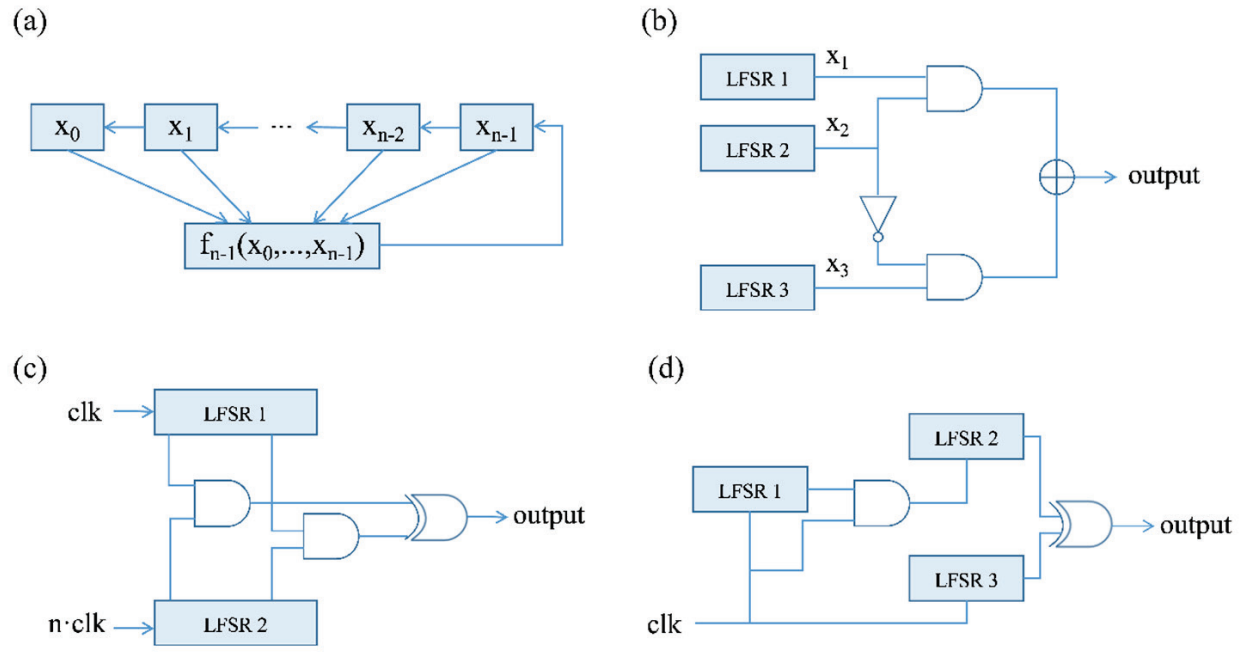

Fig. S8 Four types of NFSR designs. **(a)** n-bit Fibonacci NFSR. **(b)** Geffe generator. **(c)** Massey-Rueppel multispeed generator. **(d)** Beth-Piper generator.

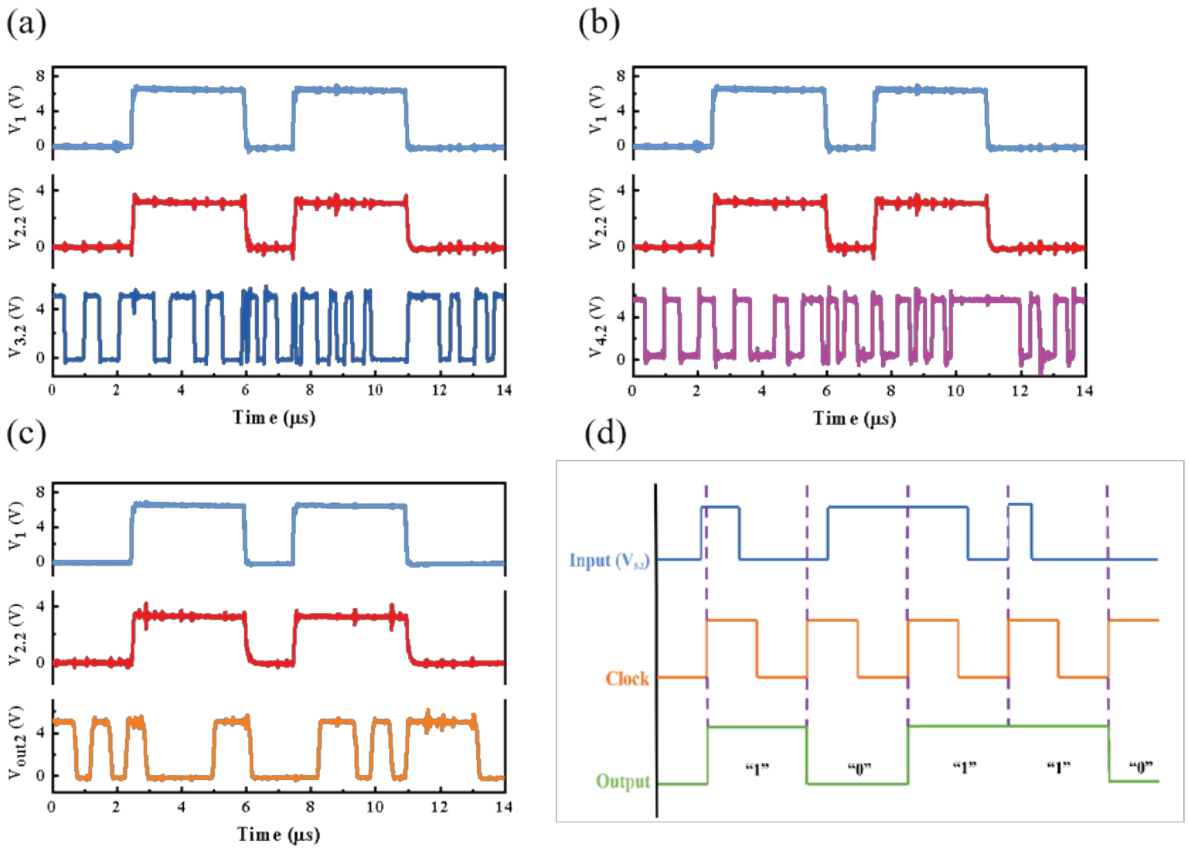

Fig. S9 Implementation of the TRNG of the right circuit. **(a, b)** Voltage test results of each test node. **(c)** Measured

output results of two continuous periods of TRNG. **(d)** TRNG output demonstration process.

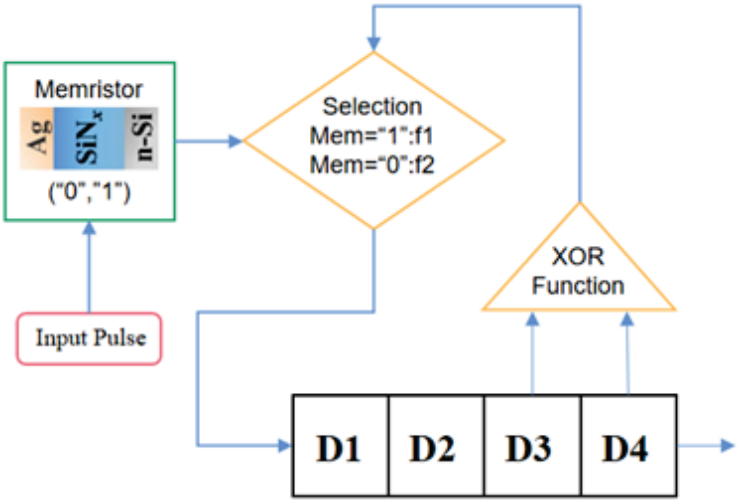

Fig. S10 Schematic diagram of circuit working principle.

Table S1 Analog operating truth table.

D1	D2	D3	D4	f1(D1,D2,D3,D4)	Memristor	f2(D1,D2,D3,D4)
1	0	0	0	0	1	0
0	1	0	0	0	1	0
0	0	1	0	1	1	1
1	0	0	1	0	0	1
1	1	0	0	0	0	1
1	1	1	0	1	0	0
0	1	1	1	0	1	0
.....						

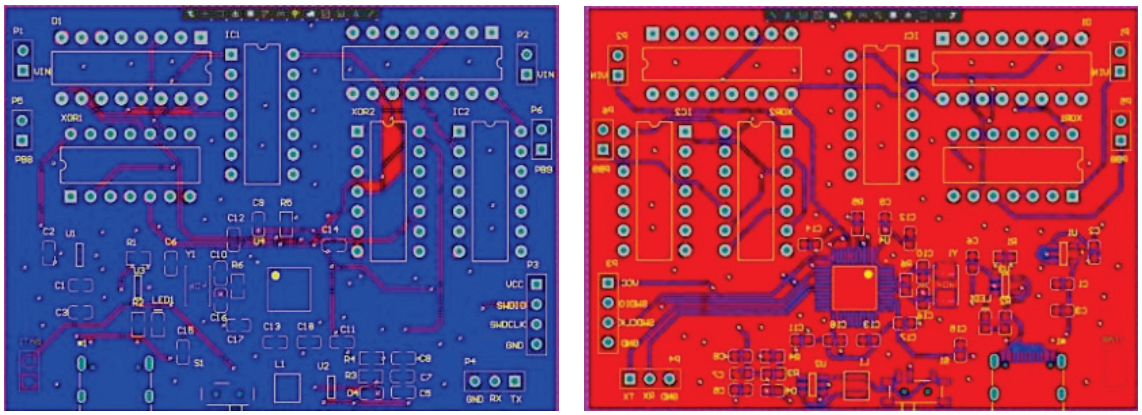

Fig. S11 PCB layout.

Table S2 Comparison of variation [$\delta=\Delta V(2\sigma)/V_{mean}$] of TS devices.

Material system	δ_{th}	δ_{h}	Reference
Ag/SiC/Pt	14.2 %	52.9 %	[1]
Pt/CuS/GeSe/Pt	22.4 %	-	[13]
VO_2-based MIT	50.8 %	-	[13]
TiN/HfO_2/$InGaZnO_4$/Si	26.5 %	42.9 %	[16]
Ag/SiN_x/n-Si	9.1 %	23.0 %	This work

Table S3 Comparison of switching speeds of TS devices.

Material system	Turn-on time	Turn-off time	Reference
Cu/TaO_x/δ-Cu/Pt	70 ms	no	[8]
Cu/SiO_2/Pt	4 ms	＜1ms	[9]
Ag/SiO_x/C	~5 μs	~20 μs	[10]
Ag/HfO_2/SiO_2/p^+-Si	~58 ns	~67 ns	[11]
Pd/Ag/HfO_x/Ag/Pd	＜75 ns	＜250 ns	[12]
Pt/CuS/GeSe/Pt	~200 ns	~3 μs	[13]
Pt/Ag/TiN/$HfAlO_x$/Pt	~50 ns	~500 ns	[14]
Pt/Ag/Ag: SiO_2/Pt	~55 μs	~60 μs	[7]
Ag/WSe_2/Ag	~700 ns	~300 ns	[15]
Ag/SiN_x/n-Si	~47 ns	~38 ns	This work

References

[1] L. A. Liu, J. H. Zhao, G. Cao, S. K. Zheng, and X. B. Yan, *Adv. Mater. Technol.* 6, 2100373 (2021)

[2] Y. H. Chen, Y. Wang, Y. H. Luo, X. W. Liu, Y. Q. Wang, F. Gao, J. G. Xu, E. T. Hu, S. Samanta, X. Wan, X. J. Lian, J. Xiao, and Y. Tong, *IEEE Electron Device Lett.* 40, 1686 (2019)

[3] L. G. Gao, F. Alibart, and D. B. Strukov, *IEEE Trans. Nanotech.* 12, 115 (2013)

[4] L. Yan, Y. F. Pei, J. J. Wang, H. He, Y. Zhao, X. Y. Li, Y. X. Wei, and X. B. Yan, *Appl. Phys. Lett.* **119** (15), 153507 (2021)

[5] J. Yoo, J. Woo, J. Song, and H. Hwang, *AIP Adv.* 5, 127221 (2015)

[6] Z. Zhou, X. Yan, J. Zhao, C. Lu, D. Ren, N. Lu, J. Wang, L. Zhang, X. Li, and H. Wang, *J. Mater. Chem. C* 7, 1561 (2019)

[7] Z. R. Wang, S. Joshi, S. E. Savel'ev, H. Jiang, R. Midya, P. Lin, M. Hu, N. Ge, J. P. Strachan, Z. Y. Li, Q. Wu, M. Barne, G. L. Li, H. L. Xin, R. S. Williams, Q. F. Xia, and J. J. Yang, *Nat. Mater.* 16, 101 (2017)

[8] T. Liu, M. Verma, Y. Kang, and M. Orlowski, *Appl. Phys. Lett.* 101, 073510 (2012)

[9] W. Chen, H. Barnaby, and M. Kozicki, *IEEE Electron Device Lett.* 37, 580 (2016)

[10] A. Bricalli, E. Ambrosi, M. Laudato, M. Maestro, R. Rodriguez, and D. Ielmini, *IEEE Trans. Electron Devices* 65, 122 (2017)

[11] Y. Lee, C. Mahata, M. Kang, and S. Kim, *Appl. Surf. Sci.* 565, 150563 (2021)

[12] R. Midya, Z. Wang, J. Zhang, S. E. Savel'ev, C. Li, M. Rao, M. H. Jang, S. Joshi, H. Jiang, P. Lin, K. Norris, N. Ge, Q. Wu, M. Barnell, Z. Li, H. L. Xin, R. S. Williams, Q. Xia, and J. J. Yang, *Adv. Mater.* 29, 1604457 (2017)

[13] K. Wang, Q. Hu, B. Gao, Q. Lin, F. W. Zhuge, D. Y. Zhang, L. Wang, Y. H. He, R. H. Scheicher, H. Tong, and X. S. Miao, *Mater Horiz.* 8, 619 (2021)

[14] Y. F. Lu, Y. Li, H. Y. Li, T. Q. Wan, X. D. Huang, Y. H. He, and X. S. Miao, *IEEE Electron Device Lett*. 41, 1245 (2020)

[15] M. Sivan, Y. D. Li, H. Veluri, Y. S. Zhao, B. S. Tang, X. H. Wang, E. Zamburg, J. F. Leong, J. X. Niu, U. Chand, and A. V. Y. Thean, *Nat. Commun.* 10, 1 (2019)

[16] Y. X. Zhang, Z. L. Fang, and X. B. Yan, *Appl. Phys. Lett*. 120, 213502 (2022)